Journal of Materials Science (2016) 16 pages
DOI: 10.1007/s10853-016-9879-6

B2 long-range order in mechanically alloyed $Fe_{53.3-0.6x}Co_{46.7-0.4x}Sn_x$ ($2 \leq x \leq 26$) annealed at moderate temperatures

B. Malaman[1], G. Le Caër[2,*], B.F.O. Costa[3]

[1] Institut Jean Lamour, Département P2M, Equipe 103, CNRS (UMR 7198)- Université de Nancy, B.P. 70239, 54506 Vandoeuvre-les-Nancy Cedex, France
[2] Institut de Physique de Rennes, UMR UR1-CNRS 6251, Université de Rennes I, Campus de Beaulieu, Bat 11A, 35042 Rennes Cedex, France
[3] CFisUC, Physics Department, University of Coimbra, 3004-516 Coimbra, Portugal

** Corresponding author: gerard.le-caer@univ-rennes1.fr*

Received: 6 December 2015
Accepted: 3 March 2016
Published on line: 15 March 2016

Abstract: Recent interest in Fe-Co-Sn alloys stems from Heusler alloys. A Co2FeSn Heusler alloy is found to be unstable relative to other phases from ab initio calculations. However, it may be synthesized by non-equilibrium techniques. The present work focuses similarly on metastable ordered phases in ternary Fe-Co-Sn alloys. First, disordered phases of Sn in near-equiatomic Fe-Co are prepared by high-energy ball-milling. As-milled powders are then annealed to possibly produce long-range ordered phases. As-milled powders, of overall composition $Fe_{53.3-0.6x}Co_{46.7-0.4x}Sn_x$ ($2 \leq x \leq 34$), consist of a single supersaturated bcc phase for x<~15 at.%. For larger values of x, they are primarily composed of a bcc phase, whose tin content still increases up to ~26 at.%, and of extra phases, which include hexagonal $(Fe,Co)_3Sn_2$. Neutron diffraction patterns and ^{119}Sn Mössbauer spectra prove that bcc phases of as-milled alloys order to CsCl (B2) type structures for $x \leq 26$ when annealed at 673K. In addition, ^{119}Sn Mössbauer spectra reveal that a Sn content of ~15 at.% marks the separation between domains with different short-range orders. From previous and present results, metastable B2 ordering of Sn-rich Co-Fe-Sn alloys is concluded to occur over a significant concentration range.

Keywords: Fe-Co-Sn alloys, Heusler alloys, mechanical alloying, B2 long-range order, Mössbauer spectroscopy

1. Introduction

Near-equiatomic $Fe_{100-x}Co_x$ alloys, which are body-centered cubic (bcc), denoted as A2, between ~1000K and ~1250K, order to a CsCl type structure (B2) at temperatures below ~1000K for x ranging between ~40 and ~60 [1]. A perfect B2 FeCo alloy may be described as two interpenetrating simple cubic sublattices, in (0,0,0) and in (1/2,1/2,1/2), Fe on one and Co on the other. Ferromagnetism stabilizes the B2 phase of Fe-Co alloys [2-3] and the bcc phase of Fe at low temperature [4]. In addition, magnetism plays a crucial role in the formation of point defects in B2 FeCo. It results in an effective formation energy of thermal antisite defects which is much smaller than those of Fe and Co vacancies [2]. Cooling rates of at least ~4000K/s are needed to bypass the order-disorder transformation of equiatomic FeCo, i.e. to retain the high-temperature disordered bcc phase at low temperature [1]. Such rates can only be achieved by ultrafast quenching [5].

The B2 unit cell may serve as a basic brick for the construction of other ordered structures, in particular those of ternary alloys like half-Heusler (XYZ, C1b structure) and Heusler (X_2YZ, $L2_1$ structure) alloys [6], where X and Y are transition metal elements, notably 3d elements, and Z is a sp element. The structures of Heusler and half-Heusler can be described from four interpenetrating fcc sublattices, one being empty in half-Heusler alloys.

1.1 Ternary Fe-Co-Sn alloys; Heusler and related alloys

Until recently, the Fe-Co-Sn system was essentially uninvestigated. The compound FeCoSn, with a hexagonal Ni_2In type structure, was however studied in [7]. Splat-quenched alloys $Fe_{75-x}Co_xSn_{25}$ ($0 \leq x \leq 75$) were reported to be B2 for any x [8]. On the contrary, splat-quenched $Co_{75}Sn_{25}$ was found to be A2 [9]. Further, splat-quenched $Fe_{35}Co_{40}Sn_{25}$ annealed for 12h at 1073K and water quenched was reported to consist of hexagonal Co_3Sn_2 and of bcc Fe(Sn) [8], most likely bcc (Fe-Co) as found hereafter for $Fe_{38}Co_{36}Sn_{26}$ (sections 3 and 4). Recent interest in Fe-Co-Sn alloys stems from Heusler alloys because of the magnetic properties of this class of materials and the associated functional properties, for instance, shape memory, magnetocaloric effect, magnetoresistance, thermoelectric power, spintronic [6].

Ordered alloys of the ternary systems Co-Mn-Sn and Ni-Mn-Sn are interesting, more particularly in relation with Heusler alloys. The structures of quaternary $Co_2Mn_{1-x}Fe_xSn$ alloys, prepared by arc-melting, were studied by Zhang et al. [10]. Heusler alloys are formed for x ranging from 0 to 0.5 while the alloys phase separate into Co_3Sn_2, presumably hexagonal, and bcc Fe-Co for x>0.5. A Co_2FeSn Heusler alloy is concluded to be unstable relative to other phases from ab initio calculations [6]. The alloy Co_2FeSn, formed by high temperature direct synthesis calorimetry, is for instance decomposed into Co_3Sn_2 and bcc Fe-Co [11]. The energy difference is however relatively small so that a Co_2FeSn Heusler phase is concluded to be possibly synthesized by non-equilibrium techniques [6]. The latter difference is more unfavorable to the formation of a Fe_2CoSn Heusler alloy [6]. Most recent studies of ternary Fe-Co-Sn alloys concentrate therefore on Co_2FeSn. Three types of alloy structures have been reported according to the preparation method, bcc (A2), B2 and $L2_1$. Ternary Fe-Co-Sn alloys were prepared by electrodeposition: as-prepared alloys, among which Co_2FeSn and alloys whose compositions are close to those investigated here (section 1.3), were established to be bcc (A2) [12-13]. Small amounts of Co_3Sn_2 were observed to form according to the current densities [12]. Li et al. used a reduction method of metal chlorides and sulfate, with sodium hypophosphite as a reducing agent, to prepare nanoparticles of B2 Co_2FeSn [14]. Finally, $L2_1$ Co_2FeSn Heusler alloys films were synthesized by atomically controlled deposition of successive layers of Co, Fe and Sn for substrate temperatures of at most 523K [15]. The present work is more particularly focused on metastable ordered alloys prepared by annealing of disordered phases of Sn in near-equiatomic Fe-Co made by mechanical alloying. General characteristics of the latter non-equilibrium technique are summarized below [16-17].

1.2 Mechanical alloying and grinding

Mechanical alloying of mixtures of powders of pure elements or of powders of already partially combined elements is basically a dry and high-energy milling process used to synthesize all kinds of materials, often with non-equilibrium structures, from metallic to ionic such as extended solid solutions, alloys of immiscible elements, amorphous phases, all sorts of compounds and composites [16-17]. Mechanical grinding differs from mechanical alloying in that the chemical composition of the starting powder particles remains the same during milling but their structure is expected to evolve.

In the mechanical alloying process of ductile elemental powder mixtures, particles are trapped between colliding balls or between balls and vial. They are subjected to a severe plastic deformation, which exceeds their mechanical strength, accompanied by a temperature rise. Particles are repeatedly flattened, fractured and welded. A layered structure of the ground elements is formed initially. It is progressively refined and becomes tortuous. Fracture and welding are the two essential events through which matter is permanently exchanged between particles. They ensure mixing of the elements of ground powders down to the atomic scale.

Milled powders of a given composition reach a stationary state, or dynamical equilibrium, through the combined action of plastic deformation and of diffusion for given mechanical and thermal working conditions of the high-energy mill as advocated in the theory of driven systems applied to ball-milling [18]. The phases which are expected to form depend on the milling conditions whose parameters for the present study are described in section 2. An example relevant to the present work is that of grinding of B2 FeAl in a Fritsch P0 vibratory mill which consists of a tungsten carbide vial vibrating at 50 Hz [19]. The vial contains a single ball either a 1 kg tungsten carbide ball or a 500 g hardened steel ball and powders. The FeAl equilibrium structure is of the B2 type up to its melting temperature which exceeds 1500K. A dynamical diagram gives the steady state value of the LRO parameter S as a function of milling temperature for a given "milling intensity" (figure 7 of [19]). The latter is defined by Pochet et al. to be equal to $M_b V_{max} f/M_p$ with M_b the mass of the ball, V_{max} the maximum velocity of the ball, f the impact frequency and M_p the mass of powder in the vial. At room temperature (RT) and below, the steady state structure is disordered bcc (figure 7 of [19]). Between RT and ~530K, the LRO parameter increases progressively up to S=1. The steady state results from a competition between atomic jumps forced by shear and thermal jumps. Disorder induced by shear dominates at low temperature and explains that B2 FeAl transforms by ball-milling into a disordered bcc phase. Experiments were not performed at temperatures higher than ~530K.

In all experiments described below, high-energy ball-mills operate at RT. For convenience, we denote hereafter as p-$A_xB_yC_z$ an initial mixture of elemental powders of composition $A_xB_yC_z$ to be milled. The compositions of as-milled powders differ in

general from the initial ones as elements from milling tools, notably iron, are incorporated into the milled powders.

1.3 Nanocrystalline mechanically alloyed p-$Fe_{50-y/2}Co_{50-y/2}Sn_y$

In classical milling conditions, similar to those used here (section 2), disordered bcc FeCo forms either by mechanical alloying of initial powder mixtures of elemental Fe and Co at RT [20–24] or by grinding B2 FeCo at RT for only 90 minutes [25]. In the latter case, shear-induced disorder dominates, as above, the trend towards ordering. The stationary state of as-milled B2 FeCo consists then of a disordered bcc phase, with a typical crystallite size of ~10 nm [25]. This stationary state does not depend on the nature of starting powders (alloyed or not).

The solubility of Sn in FeCo (A2 or B2) is very low at equilibrium, ~ 1 at% [26-28]. High-energy ball-milling is a possible method to enhance it. Mechanical alloying was employed to synthesize ternary Fe-Co-Sn alloys from p-$Fe_{50-y/2}Co_{50-y/2}Sn_y$ for $y \leq 33$ at.% in the milling conditions described in section 2 [29-31]. When tin is added, a supersaturated solid solution of Sn in near-equiatomic bcc FeCo is expected to form. However, there is currently no way to predict theoretically the maximum degree of supersaturation in the given milling conditions and it is necessary to resort to experiment to determine it. The dissolution of Sn in near-equiatomic bcc Fe–Co was unambiguously proven by X-ray diffraction (figure 1) and by ^{57}Fe and ^{119}Sn Mössbauer spectroscopy (section 3.1). A disordered bcc phase, with significant amounts of tin dissolved in it, was found to remain the principal constituent of as-milled p-$Fe_{50-y/2}Co_{50-y/2}Sn_y$ alloys (figure 1). The maximum solubility of Sn in near-equiatomic nanocrystalline bcc FeCo, in the milling conditions described in section 2, is at least equal to 15±2 at.%. The difficulty raised by its determination is discussed in section 4.1.

1.4 Ordering of mechanosynthesized nanocrystalline alloys and aims

The combination of mechanical alloying and of annealing at moderate temperatures is a possible method to follow the recovery of order in as-milled nanocrystalline alloys when their coarse-grained counterparts are ordered at equilibrium. Some examples, among many, of ordered alloys disordered by ball-milling whose order is re-established by subsequent annealing, are $L2_1$ Ni_2MnSn [32], $L1_2$ Ni_3Al [33] and B2 $Fe_{60}Al_{40}$ [34]. In addition, mechanical alloying followed by annealing makes possible the formation of

metastable ordered alloys from alloys which are not long-range ordered at equilibrium but are prone to ordering. An example is metastable B2 ordering of near-equiatomic bcc Fe-V nanocrystalline alloys [35]. The present study of mechanosynthesized alloys from ternary mixtures p-$Fe_{50-y/2}Co_{50-y/2}Sn_y$ ($y \leq 33$) falls within this framework.

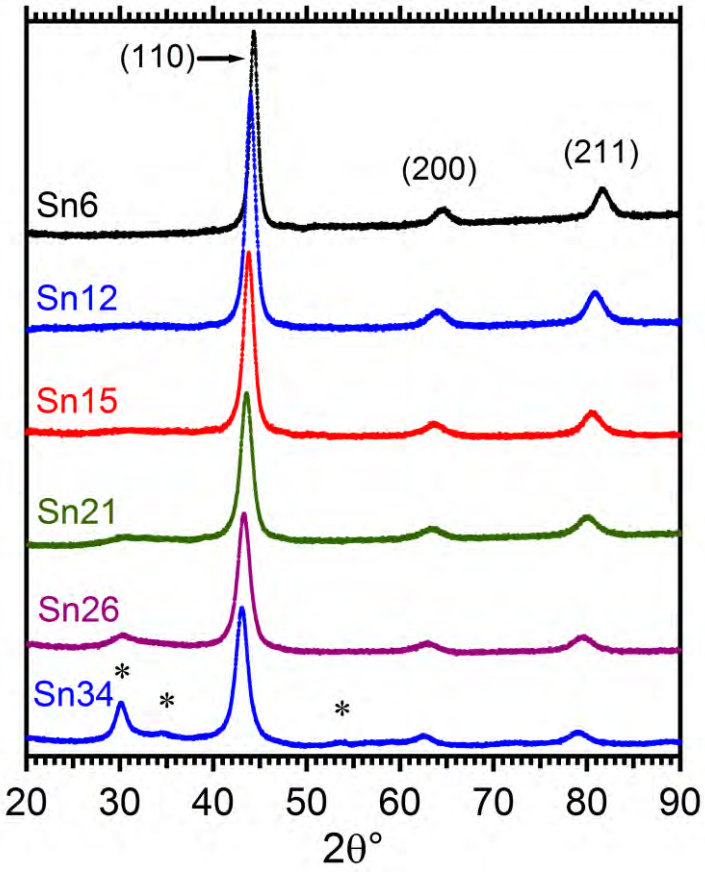


Figure 1- X-ray diffraction patterns of as-milled (10h) $Fe_{53.3-0.6x}Co_{46.7-0.4x}Sn_x$ for the indicated tin contents (Cu Kα, λ =0.1542 nm). The most significant peaks of hexagonal $(Fe,Co)_3Sn_2$ ($B8_2$-type) are shown by asterisks. (color online)

The sole or preponderant constituent of as-milled powders is a metastable bcc phase ([29-31] and figure 1). The question then arises as to whether metastable tin-rich bcc phases do order to a B2 structure when annealed as do stable dilute solutions of tin in bcc FeCo [26-28] and, if so, what is the range of tin content in which B2 ordering occurs. The peculiarities of annealing of nanocrystalline alloys, are essential for this purpose. Their high density of defects, in particular vacancies and grain boundaries, enhance the kinetics of ordering when they are annealed at moderate temperatures. The ordering of nanocrystalline alloys can thus be studied at lower temperatures and more

practical times than would coarse-grained alloys [35]. However, the maximum steady-state value of the long-range order (LRO) parameter S they reach is typically ~80% of the maximum value measured in their microcrystalline counterparts ([35] and references therein).

The present paper aims to study the transformations of p-$Fe_{50-y/2}Co_{50-y/2}Sn_y$ powder mixtures ($y \leq 33$) ball-milled at high-energy and then annealed at moderate temperatures. Two techniques, neutron diffraction and ^{119}Sn Mössbauer spectroscopy, are essential to evidence the emergence of B2 long-range order in annealed powders. We first recall the main structural features of p-$Fe_{50-y/2}Co_{50-y/2}Sn_y$ ($y \leq 33$) blends ball-milled at high energy. Then, we describe and discuss the results of an experimental study of annealed alloys by neutron diffraction and by ^{57}Fe and ^{119}Sn Mössbauer spectroscopy.

2. Experimental

Elemental powder mixtures of Fe (purity: 99.9%), Co (purity: 99.8%) and Sn (purity: 99.5%) were ball-milled in argon atmosphere for 10h in a planetary Fritsch P6 ball-mill operating at RT at a disc rotation speed of 500 rpm. The rotating disc of the mill bears a vial which rotates in the opposite direction. The vial contains seven balls of 15 mm diameter and the powder mixture to be milled. Vials and balls are made of hardened steel. The powder-to-ball weight ratio was 1:20. The chosen milling time of 10h ensures that powders reach a stationary state in these dynamical milling conditions as confirmed for instance by figure 2 (see too section 3.1). Except if otherwise stated, "as-milled" stands hereafter for "milled for 10h under the above-specified conditions".

The compositions of as-milled powders were determined by energy-dispersive X-ray spectroscopy (EDS) in a scanning electron microscope JEOL JSM630, working at 15kV. The library standards provided by the instrument manufacturer (Oxford INCA Energy 350) were used for the quantitative analysis of the EDS data. The compositions of as-milled alloys deviate from their starting compositions. The final Sn content x is a little larger, by less than ~1 at.%, than the nominal content y. It is given by $x=1.05y-0.16$ with an accuracy better than 0.2 at.% for $2 \leq y \leq 25$ while $x=34$ for $y=33.3$. The Fe (rsp. Co) content is larger (rsp. smaller) than its nominal content. A Cr content less

than 0.2 at.% is neglected hereafter. The overall composition is well described by $Fe_{53.3-0.6x}Co_{46.7-0.4x}Sn_x$ where the calculated Fe and Co contents are accurate to within ~0.3 at.% for $2 \leq x \leq 26$. The alloy composition is $Fe_{34.7}Co_{31.3}Sn_{34}$ for x=34. For the sake of simplicity, while remaining still consistent with the actual precision of composition measurements, any alloy is designated hereafter by Fe, Co and Sn contents rounded to the nearest integers, for instance $Fe_{35}Co_{31}Sn_{34}$ for the latter alloy. Figures are however plotted with tin contents determined by EDS.

As-milled powders were placed in quartz tubes opened at one end. The tubes were first evacuated by a primary pump and were then filled with argon. These two steps were repeated ten times before sealing the tubes under an argon pressure of about 27 kPa at 300K which becomes ~60 kPa at 673K. As-milled alloys were finally annealed at 673K for 15h.

Annealed alloys were characterized by X-ray diffraction (XRD) using CuKα radiation ($\lambda = 0.1542$ nm). The precise determination of peak positions was carried out by means of the software Analyze-RayfleX supplied by Agfa Seifert. Lattice parameters of bcc phases (figure 2) were then obtained by least-square fitting using a cell parameter refinement software named U-FIT [36]. Neutron diffraction (ND) experiments were carried out at Institut Laue Langevin (ILL, Grenoble, France), with the one-dimensional multidetector D1B (λ =0.252 nm).

^{57}Fe and ^{119}Sn Mössbauer spectra were recorded at room temperature, in transmission geometry, by a constant acceleration type spectrometer using sources of ^{57}Co in Rh and ^{119m}Sn in $CaSnO_3$ both with a strength of ~ 10 mCi. Isomer shifts are not really relevant in the present context. When mentioned they are referenced to α-Fe at RT and to SnO_2 at RT for Fe and Sn respectively. Hyperfine magnetic field distributions (HMFD's), $P_X(B)$, were analyzed both for ^{57}Fe and ^{119}Sn with a constrained Hesse–Rübartsch method [37] employing Lorentz lines. In the previous notation, X is either F or S which stand for ^{57}Fe and ^{119}Sn respectively. Any HMFD is such that $P_X(B)dB$, represents primarily the fraction of X atoms whose field lies between B and B + dB. The mean HMF is denoted as $\langle B_X \rangle$. The 'width' of a distribution $P_X(B)$ is represented below by a standard-deviation $\sigma_X = \langle (B_X - \langle B_X \rangle)^2 \rangle^{1/2}$. Finally, we define B_M either as the ^{57}Fe HMF for which $P_F(B)$ is maximum when B ranges between ~20 and 40 T or as the ^{119}Sn HMF for which $P_S(B)$ is maximum when B ranges between ~5 and 30 T where the

context makes it clear which is which. Typical errors on $<B_X>$ and on B_M are respectively of ~0.3 T and ~0.2 T.

3. Results

3.1 Previous characterizations of as-milled $Fe_{53.3-0.6x}Co_{46.7-0.4x}Sn_x$ alloys ($x \leq 34$)

The formation of metastable bcc $Fe_{53.3-0.6x}Co_{46.7-0.4x}Sn_x$ by mechanical alloying takes place in two steps as shown by a study of a representative alloy, $Fe_{46}Co_{42}Sn_{12}$ [31]. The first stage, for milling times t_m ranging from 0.5h to 2h is characterized by the formation of stannides, $FeSn_2$ and $CoSn_5$ respectively at the Fe-Sn and Co-Sn interfaces. Solid solutions are formed at Fe-Co interfaces. Tetragonal $FeSn_2$, with a $CuAl_2$ type structure, forms too during the first stage of mechanical alloying of Fe-Sn solid solutions [38-40]. The formation and the structure of a tetragonal stannide, $CoSn_5$, prepared via a conversion chemistry route and possibly non-stoechiometric $Co_{1-z}Sn_5$ (z=0.1-0.2), were reported only recently [41]. It was shown to be non-magnetic [31]. Both stannides disappear for longer milling times, only after ~1h for $CoSn_5$.The second stage occurs for $t_m \geq 2.5$h until a stationary state is reached at $t_m \sim 8$h.

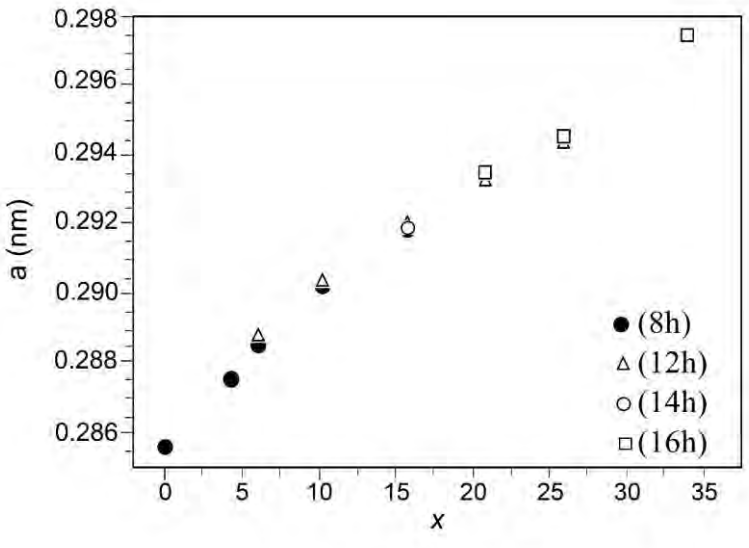


Figure 2 – Evolution with tin content of the lattice parameter of the bcc phase of as-milled $Fe_{53.3-0.6x}Co_{46.7-0.4x}Sn_x$ (milling times range from 8h to 16h).

The lattice parameter a(x) of the supersaturated bcc phase of elemental powder mixtures of composition $Fe_{53.3-0.6x}Co_{46.7-0.4x}Sn_x$ milled for times ranging from 8h to 16h is shown

in figure 2 as a function of x. It varies according to Vegard's law for $x \leq 10$ with a(0)=0.2858(1) nm and a slope of $4.61(9)10^{-4}$ nm(at.%)$^{-1}$. For larger values of x, a(x) increases steadily but deviates from Vegard's law, being for instance 0.2935(2) nm for x=21. The lattice parameters for a given x remain essentially constant for samples whose milling times range from 8h to 16h. This confirms that a stationary state, i.e. a dynamical equilibrium (section 1.2), has been reached at ~8h of milling.

XRD patterns evidence the formation of a bcc phase while well-separated peaks at ~30° grow progressively when x increases from 21 to 34 (figure 1). As mentioned in [30], the broad additional peaks would be due to nanocrystalline hexagonal Co_3Sn_2 of the $B8_2$ type with some iron dissolved in it, denoted hereafter as $(Fe,Co)_3Sn_2$. High-energy ball-milling of Co_3Sn_2 is known to transform the low-temperature orthorhombic phase into the high-temperature hexagonal phase ($P6_3/mmc$) [42]. However, the XRD pattern (CuKα) of amorphous Co_3Sn_2, prepared by a solvothermal route, exhibits also a broad halo at ~32° and a second one at ~43° [43] which corresponds here to the position of the (110) peak of the bcc phase (fig.1). Haloes are observed as well at 32° and 43° in electro-co-deposited $Co_{33}Sn_{67}$ [44]. The formation of amorphous Co-Sn alloys by solid-state diffusion in multilayers or in granular systems is known to take place at room temperature because cobalt is a fast diffuser when dissolved into tin [45-46]. Gaffet et al. [46] report that amorphous $Co_{100-z}Sn_z$ decomposes for long diffusion times at RT and forms Co_3Sn_2 for $0<z\leq35$. We identified too hexagonal $(Fe,Co)_3Sn_2$ from narrower peaks of XRD patterns of as-milled samples annealed in the range 673-773K. The formation of a Co-rich (Fe,Co)-Sn amorphous phase, partly crystallized, provides thus a plausible explanation of the systematic presence, for high tin contents, of diffraction peaks, at ~30°, which are asymmetrical with slowly decreasing right tails (figure 1, x=21,26). The presence of crystalline $(Fe,Co)_3Sn_2$ is clearly exhibited by the XRD lines at ~30° for x=21, 26, 34 (figure 1).

3.2 As-milled alloys: neutron diffraction and Mössbauer spectroscopy

Representative neutron diffraction patterns of as-milled alloys are shown in figure 3 for four values of x and 2θ ranging from 20° to 110°. They focus on the angular range in which superlattice lines are expected to appear clearly in annealed alloys and on the (110) line of the bcc phase. Only very small peaks at ~35° and small bumps are

observed at ~50° for x=21, 26. The peak shift towards smaller angles when x increases reflects the associated increase of the lattice parameter (figure 2).

Figure 4 shows representative RT ^{57}Fe and ^{119}Sn Mössbauer spectra of as-milled alloys. The mean ^{57}Fe hyperfine magnetic field at room temperature $\langle B_F(x)\rangle$ decreases fairly linearly with x, $\langle B_F(x)\rangle$ (T) = 34.7-0.25x. The field $\langle B_F(0)\rangle$=34.7 T is consistent with the HMF's measured in mechanically alloyed FeCo which are all reported to be close to 35 T [19-23]. The mean ^{57}Fe isomer shift of as-milled bcc alloys increases rather linearly from 0.06(4) mm/s for x=0 to 0.20(4) mm/s for x=26 [30]. The rate of decrease of the mean ^{57}Fe HMF is comparable to the one measured in supersaturated bcc $Fe_{100-x}Sn_x$, $\langle B_F(x)\rangle \approx$ 33.1-0.30x (T) ($0 \le x \le 30$) [38]. Diamagnetic Sn reduces the average Fe HMF when dissolved in bcc FeCo as it does in bcc Fe. Further, the Curie

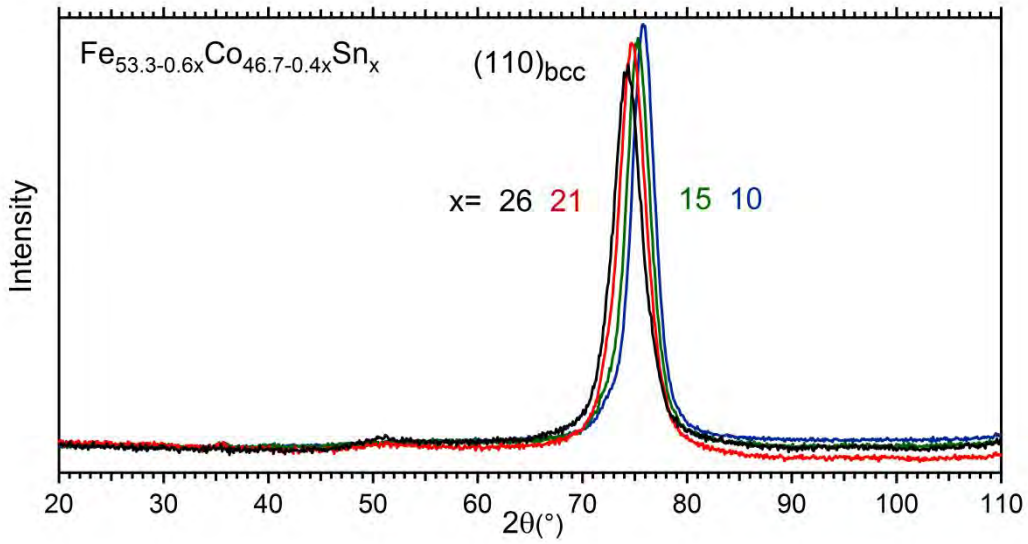


Figure 3 - Neutron diffraction patterns (λ =0.252 nm) of as-milled (10h) $Fe_{53.3-0.6x}Co_{46.7-0.4x}Sn_x$ for the indicated values of x (x increases from right to left). (color online)

temperature is expected to decrease with x rather in the same way as it does in bcc Fe-Sn [39,47].

^{119}Sn Mössbauer spectra of as-milled $Fe_{53.3-0.6x}Co_{46.7-0.4x}Sn_x$ at RT (figure 4 right) consist of a major magnetic component with two broad unresolved lines and of a minor central non-magnetic component whose weight increases with x, more particularly for x>15. The mean ^{119}Sn hyperfine magnetic field of the magnetic component remains

fairly constant for x≤15, <B_S(x)>=9.5(0.3) T [30]. It is 8.5 T for x=21.

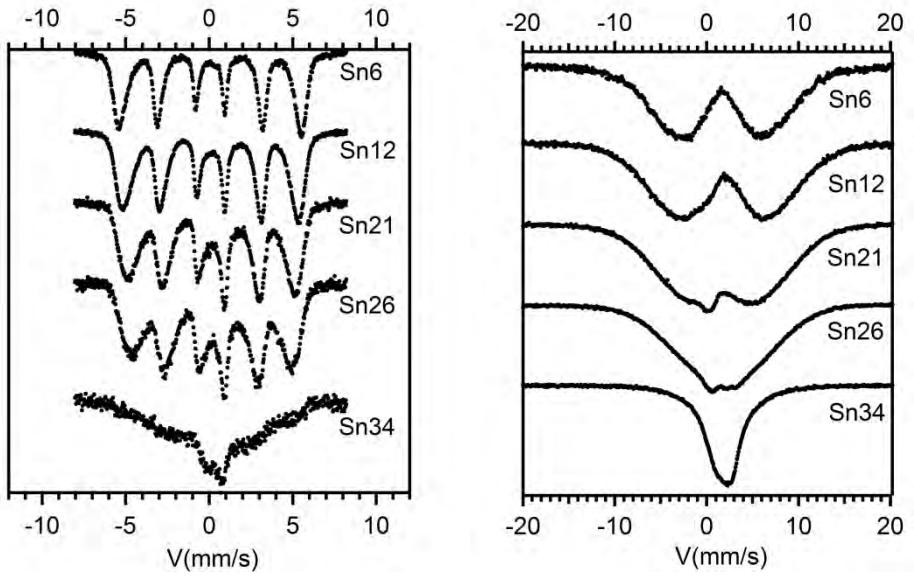


Figure 4 - RT ^{57}Fe Mössbauer spectra (left) and ^{119}Sn Mössbauer spectra (right) of as-milled (10h) $Fe_{53.3-0.6x}Co_{46.7-0.4x}Sn_x$ for the indicated values of x.

3.3 Annealed $Fe_{53.3-0.6x}Co_{46.7-0.4x}Sn_x$ ($x \leq 34$)

3.3.1 Choice of an annealing temperature

Various alloys were annealed, most often for short times, at moderate temperatures ranging typically from 673K to 873K to select an annealing temperature valid for all tin contents. For instance, the XRD patterns of $Fe_{53.3-0.6x}Co_{46.7-0.4x}Sn_x$ annealed at 623K for 15 min remain unchanged for x=10, 12, 21, 34 except for line narrowing due to crystallite growth and for the formation of a small amount of $CoFe_2O_4$. The XRD pattern of $Fe_{41}Co_{38}Sn_{21}$ annealed for 12h at 723K shows the presence of the previous oxide, of an intermetallic compound (Fe,Co)Sn of the B35 type and of a bcc alloy whose ^{57}Fe HMF is ~34.9 T. The latter field reveals that Sn atoms have been expelled from near-equiatomic bcc FeCo as expected from the low equilibrium solubility of Sn in FeCo [26-28].

Figure 5 presents XRD patterns of $Fe_{46}Co_{42}Sn_{12}$ in the as-milled state and after annealing for 35 min at 673K and for 15 min at 873K. Only minor changes are noted for the sample annealed at 673K (the peak at 35° is due to $CoFe_2O_4$ [48]). The sample annealed at 873K is decomposed. The XRD lines are due to three intermetallic

compounds, hexagonal B35 (Fe,Co)Sn, hexagonal $(Fe,Co)_3Sn_2$ of the $B8_2$ type, tetragonal C16 $(Fe,Co)Sn_2$ and to a bcc FeCo alloy. The diffraction lines of the intermetallic compounds are labeled in figure 5. The bcc alloy is depleted in Sn as shown by line shifts which result from a smaller lattice parameter. Finally, we chose a rather low annealing temperature, 673K, to prevent alloy decomposition and an annealing time of 15h.

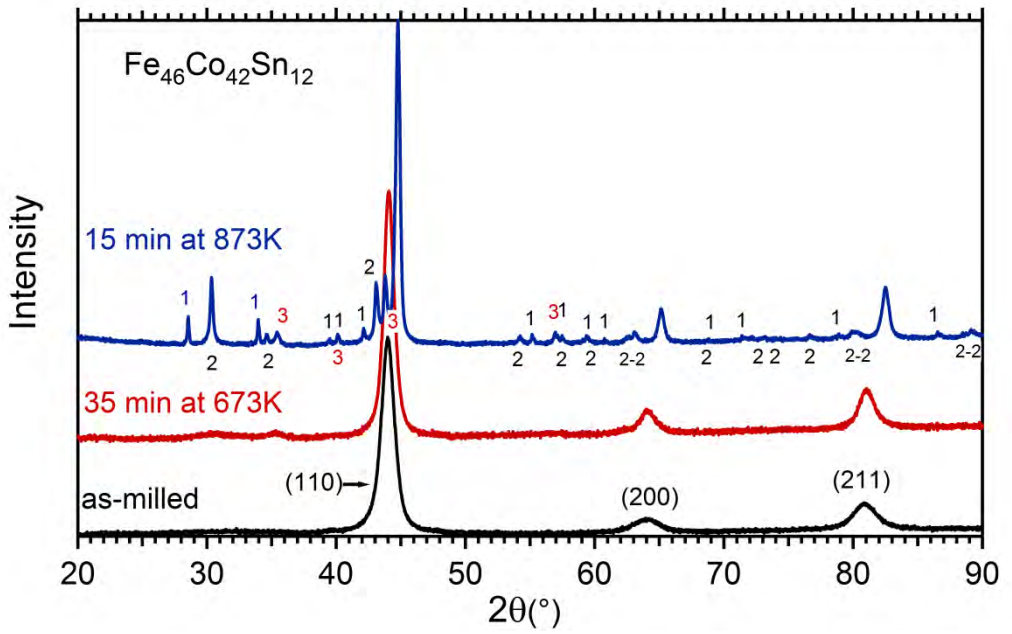


Figure 5- X-ray diffraction patterns of as-milled (10h) $Fe_{46}Co_{42}Sn_{12}$ annealed at two temperatures (1= hexagonal B35 (Fe,Co)Sn, 2=hexagonal $(Fe,Co)_3Sn_2$, 3=tetragonal C16 $(Fe,Co)Sn_2$). (color online)

3.3.2 Neutron diffraction patterns of annealed samples

Neutron diffraction patterns are displayed in figure 6 for $Fe_{53.3-0.6x}Co_{46.7-0.4x}Sn_x$ ($6 \leq x \leq 26$) alloys milled during 10h and then annealed at 673K for 15h. They reveal the presence of (100) and (111) superlattice lines. The superlattice and fundamental lines are shifted towards smaller angles as the lattice parameter increases with x. A $CoFe_2O_4$ oxide is further evidenced on neutron diffraction patterns (figure 6) because the neutron coherent scattering length of oxygen is large, b_O =5.803 fm. As expected, the oxide peak positions don't change with x. The formation of $CoFe_2O_4$ is further confirmed by small peaks at ~8 mm/s on ^{57}Fe Mössbauer spectra (figure 7, [48]). For x=34, as-milled samples decompose already when annealed for 30 min. ^{57}Fe and ^{119}Sn Mössbauer spectra, the associated HMFD's and two of their characteristics, $\langle H_X \rangle$ (X=F,S) and H_M (section 2), are shown in figures 7 to 11.

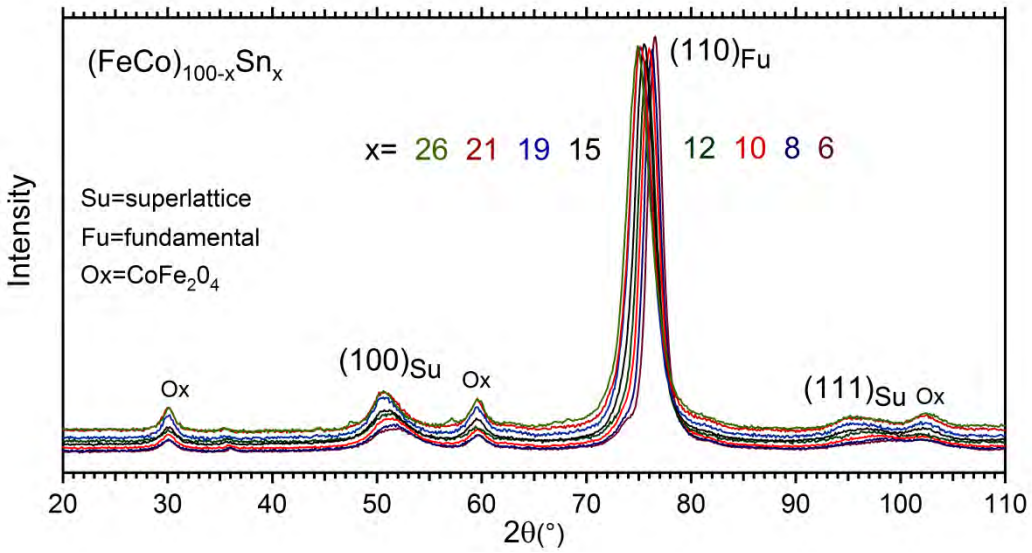


Figure 6 - Neutron diffraction patterns (λ =0.252 nm) of as-milled $Fe_{53.3-0.6x}Co_{46.7-0.4x}Sn_x$ ($6 \leq x \leq 26$) annealed at 673K for 15h. (color online)

3.3.3 ^{57}Fe Mössbauer spectra of annealed samples

Only limited changes of ^{57}Fe Mössbauer spectra occur after annealing for $x \leq 26$ (figure 7). Lines are narrower for the annealed alloys than they are for the as-milled ones and the widths of the HMFD's are thus smaller (figure 9 right for x=12). The mean HMF

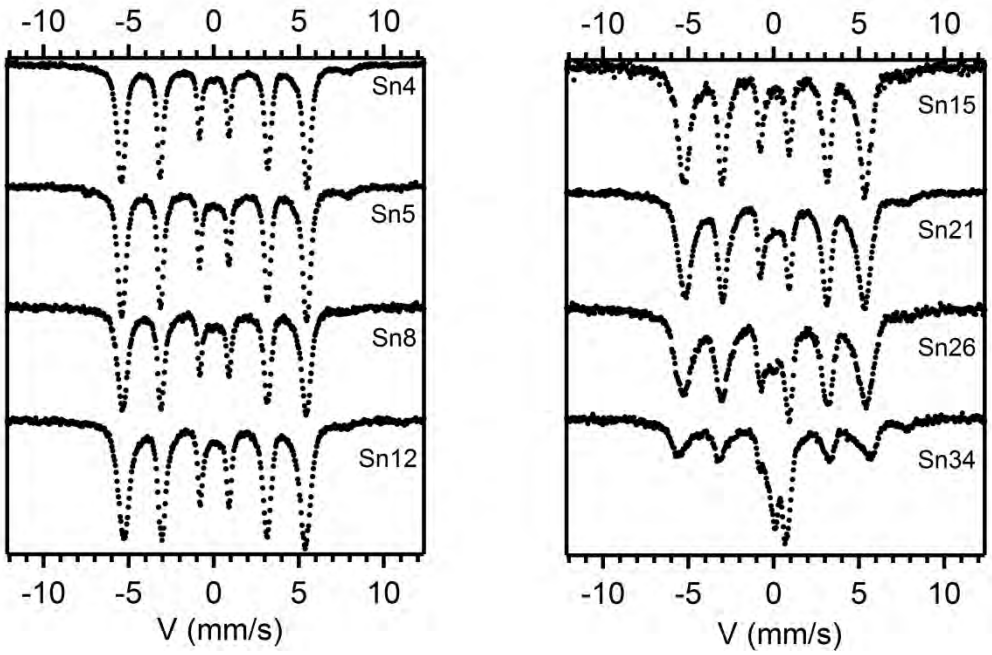


Figure 7 - RT ^{57}Fe Mössbauer spectra of as-milled (10h) $Fe_{53.3-0.6x}Co_{46.7-0.4x}Sn_x$ annealed at 673K for 15h.

for x=12 increases for instance from 31.7 T in the as-milled state to 32.9 T after annealing while the standard-deviation decreases from 3.0 T to 2.6 T. The average ^{57}Fe HMF of $Fe_{53.3-0.6x}Co_{46.7-0.4x}Sn_x$ annealed alloys ($4 \leq x \leq 26$) decreases fairly linearly when the Sn content increases, $\langle B_F(x) \rangle = 34.1\text{-}0.10x$ (T) (figure 11 left), but less rapidly than it does for as-milled alloys, $\langle B_F(x) \rangle = 34.7\text{-}0.25x$ (T). Concomitantly, the concentration dependence of the ^{57}Fe HMF B_M is well accounted for by $B_M(x) = 35.0\text{-}0.19x$ (T) in the as-milled state and, for annealed alloys, by $B_M(x) = 34.5\text{-}0.11x$ (T) and 32.6 T when $2 \leq x \leq 15$ and $15 < x \leq 26$ respectively (figure 11 left).

3.3.4 ^{119}Sn Mössbauer spectra of annealed samples

By contrast to ^{57}Fe HMF's, ^{119}Sn HMF's show a great sensitivity to chemical order when dissolved in B2 FeCo (section 4.4). The characteristics of Mössbauer spectra of annealed alloys (figure 8) differ strongly from those of their as-milled counterparts

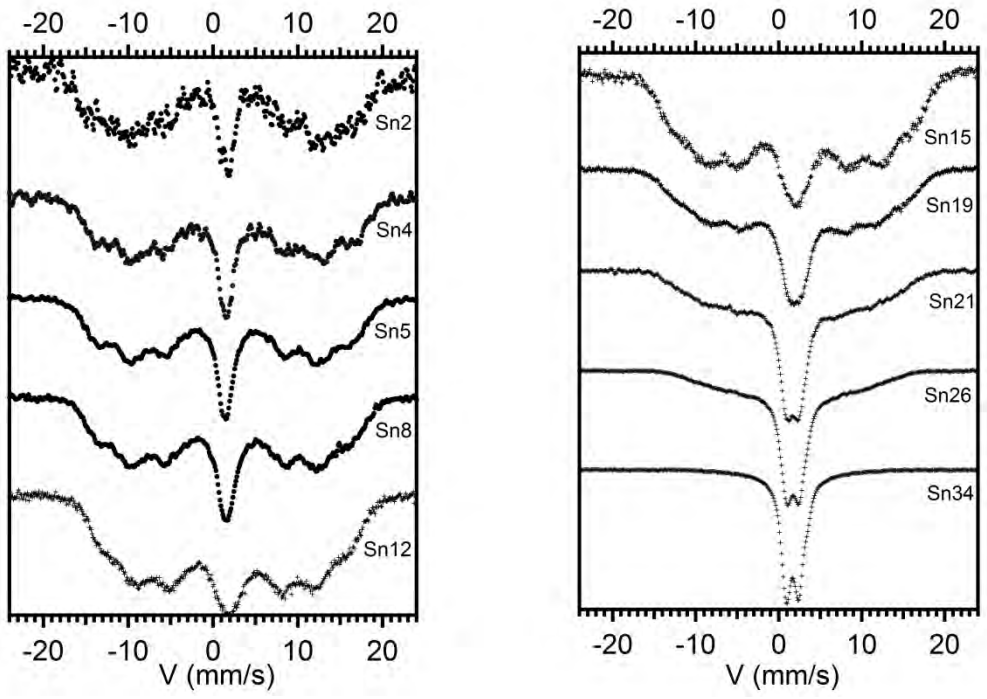


Figure 8 - RT ^{119}Sn Mössbauer spectra of as-milled (10h) $Fe_{53.3-0.6x}Co_{46.7-0.4x}Sn_x$ annealed at 673K for 15h.

(figure 4 right). They include a central component, which is the prominent feature for $x \geq 21$, while the salient characteristic is a broad magnetically split "sextet" which looks essentially unchanged for $x \leq 15$ (figure 8). Figure 9 (left) compares ^{119}Sn HMFD's of as-milled and of annealed powders for x=12. The former HMFD is approximatively

Gaussian with $<B_S(12)>\approx B_M(12)=9.8$ T and a standard-deviation of 4.8 T. The latter is split in two main peaks, one at ~1.5 T and a broad peak with B_M~20.6 T. The resulting mean HMF is then 13.6 T for annealed $Fe_{46}Co_{42}Sn_{12}$.

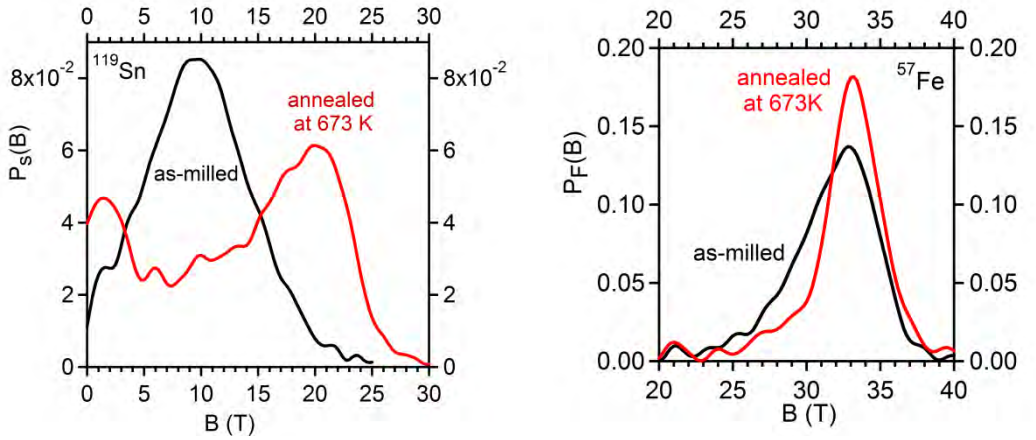


Figure 9 - RT hyperfine magnetic field distributions (^{119}Sn: left, and ^{57}Fe: right) of $Fe_{46}Co_{42}Sn_{12}$: in the as-milled state (10h) and after annealing at 673K for 15h. (color online).

4. Discussion

4.1 The solubility of tin in as-milled bcc $Fe_{53.3-0.6x}Co_{46.7-0.4x}Sn_x$

The maximum solubility x_S, in our milling conditions, of Sn in near-equiatomic nanocrystalline bcc $Fe_{53.3-0.6x}Co_{46.7-0.4x}Sn_x$ ought to be defined classically as the Sn content below which as-milled alloys are bcc and single-phase. A tentative estimate of x_S would then be 15±2 at.% (figure 1). However, the lattice parameter of the bcc phase increases gently and regularly with the Sn content even when phases co-exist with it. A clear change of slope is observed only for $x \approx 26$ (figure 2). Extra peaks become for instance more and more visible on the X-ray diffraction patterns of figure 1 and on the ^{119}Sn Mössbauer spectra of figure 4 for $x \geq 21$. Concomitantly, the ^{57}Fe and ^{119}Sn Mössbauer spectra (figure 4) and the derived hyperfine magnetic field distributions of the bcc phase [30] evolve regularly with x. The faster decrease of the mean ^{57}Fe HMF's observed for x>21 (figure 4, figure 5 of [30]) is due both to the large Sn contents and to the ensuing decrease of the Curie temperature, as observed for instance in bcc Fe-Sn [39,47] or in amorphous Fe-Sn alloys [49]. The x=34 as-milled alloy seems however to differ from those with $x \leq 26$ (see below).

A solubility, x_S=15±2 at.%, makes then the aforementioned results puzzling for $x > x_S$. The evolution of the characteristics of the bcc phase beyond the latter content requires to be interpreted from non-equilibrium features of mechanical alloying. A possible explanation relies on the external forcing action of mechanical alloying at low temperatures which drives the milled system toward composition homogenization [50]. The latter phenomenon is exemplified by mechanically alloyed binary Fe-Ni alloys (negative heat of mixing) and Fe-Cu alloys (positive heat of mixing) which exhibit similar dynamical phase diagrams ([51] and references therein). These diagrams consist of two terminal solid solutions, bcc on the Fe side and fcc on the Ni (rsp. Cu) side and, in between, of a two-phase region where the bcc and the fcc solutions have everywhere the same composition as the overall alloy. For instance, the solubility of Ni in the bcc Fe-Ni phase is not limited to the maximum Ni content of the bcc terminal solution at 15% Ni, but extends through the two-phase (bcc+fcc) region to the minimum Ni content of the fcc terminal solution at 40% [51].

A transposition of the previous idea to as-milled Fe-Co-Sn might consist of a one-phase bcc region up to ~15 at.% followed by a two-phase region (bcc+amorphous) up to ~26 at.% Sn, in which the two polymorphs would have the same composition. In addition, the amorphous phase would be partly decomposed into hexagonal $(Fe,Co)_3Sn_2$ as discussed in section 3.1 and into a bcc Fe-Co alloy. The upper tin content, ~26 at.%, is chosen here because the most marked changes take place between x=26 and x=34: a) for XRD patterns, with the sharpest 30° peak at x=34 (figure 1) b) for the composition dependence of the lattice parameter (figure 2) and c) for ^{57}Fe and ^{119}Sn Mössbauer spectra (figure 4). Finally, as-milled $Fe_{34.7}Co_{31.3}Sn_{34}$ decomposes after annealing for 30 min at 673K in contrast to as-milled powders with $x \leq 26$.

To conclude, the amount of tin which can be really dissolved in near-equiatomic bcc Fe-Co alloys in our milling conditions is certainly much closer to 26 at.% than to 15 at.%. Consistently, we show below that annealed alloys order to a B2 structure for tin contents as large as 26 at.%. The Sn content of ~15 at.% remains however remarkable in many respects (section 4.4.3).

4.2 Neutron diffraction patterns of annealed $Fe_{53.3-0.6x}Co_{46.7-0.4x}Sn_x$

The LRO parameter S of B2 $Fe_{1-z}Co_z$ is defined as $S= 2([Fe]_{Fe}-1+z)$ as the vacancy concentration is negligible [2]. Here $[Fe]_{Fe}$ is the iron concentration on the Fe sublattice

and $0 \leq S \leq 1\text{-}2\left|z\text{-}0.5\right|$ ([35] and references therein, [52]). The intensities of diffraction lines of B2 $Fe_{1-z}Co_z$ are governed by S and by f_{Fe} and f_{Co} which are respectively atomic form factors for X-ray diffraction and neutron coherent scattering lengths for neutron diffraction, generally denoted as b_{Fe} (=9.45 fm) and b_{Co} (=2.49 fm). Diffraction patterns of disordered bcc Fe-Co alloys include only fundamental (hkl) lines, with h+k+l even, while patterns of B2 ordered Fe-Co alloys include in addition superlattice lines (hkl), with h+k+l odd. The intensities of XRD fundamental lines are proportional to the square of the average form factor while those of superlattice lines are proportional to $S^2(f_{Fe}\text{-}f_{Co})^2$ [52]. Since the X-ray form factors for iron and cobalt atoms differ only slightly, the intensities of x-ray superlattice lines are nearly zero and long-range order is hardly evidenced by standard XRD. XRD with CoKα radiation might be applied to bcc Fe-Co alloys to evidence LRO through anomalous dispersion, as done for instance for B2 FeCo milled for various times [53], but neutron diffraction remains the most efficient method when accessible. In contrast to XRD, the neutron coherent scattering lengths of Fe and Co, are different enough to enable superlattice lines to appear.

In the ternary case, it would be necessary to define two long-range order parameters to describe the concentrations of Fe, Co and Sn on the two sublattices (see for instance [54]). The intensities of fundamental and superlattice lines include nuclear contributions which depend on these two LRO parameters and magnetic contributions which vary according to the considered line and represent at most ~15% of the total intensity. We will not discuss this problem further as we did not analyze line intensities. In any case, the previous discussion, valid for B2 FeCo, remains qualitatively correct in the presence of tin (b_{Sn}=6.225 fm) if the Sn repartition on the Fe and Co sublattices is random or if it is short-range ordered with diffuse scattering between Bragg peaks. It is only in the case of a long-range ordered repartition of Sn that the resulting structure would no more be B2 and that extra superlattice lines would emerge.

The presence of superlattice lines (hkl), with h+k+l odd, establishes unambiguously that the bcc phases of as-milled alloys transform, for $x \leq 26$, into long-range ordered B2 phases by annealing at moderate temperatures (figure 6). Superlattice lines are broader than fundamental lines. In the as-milled state, the crystallite size is ~6 nm. Using the Scherrer formula, we estimated the mean crystallite size and the mean size of ordered domains in annealed alloys to be respectively ~10 nm and ~4 nm. When annealed at

723K, a mechanically-alloyed bcc $Fe_{53}V_{47}$, yields similarly a B2 phase [35]. As-milled $Fe_{53}V_{47}$ powders annealed for ~20h have sizes of ordered domains, ~5 nm, which are about half those of crystallites, 9 nm (figure 5 of [35]). The latter values are comparable to those we estimate.

4.3 ^{57}Fe Mössbauer spectra of annealed $Fe_{53.3-0.6x}Co_{46.7-0.4x}Sn_x$

When a transition A2→B2 occurs in FeCo, the mean ^{57}Fe HMF decreases by an amount which depends on the long-range order parameter S [55] and is ~0.9-1 T for S=1 [56-57]. Consistently, the field $<B_F(0)>\approx$ 34.7 T for as-milled alloys is larger than the corresponding field , $<B_F(0)>\approx$ 34.1 T (section 3.3.3), for annealed alloys. A change of slope of $B_M(x)$ takes place at ~15 at.% for annealed alloys and $B_M(x)$ is essentially constant for $x \geq$ ~15 at.% (figure 11 left), a tin content which plays also a role in the evolution of ^{119}Sn spectra as discussed below.

The observed evolution of ^{57}Fe Mössbauer spectra is consistent with long-range ordering observed from neutron diffraction patterns. However, these spectra alone cannot provide convincing evidence of ordering in annealed alloys. The main contribution of ^{57}Fe Mössbauer spectroscopy is to confirm that, for $x \leq 26$, alloys consist essentially of bcc phases when as-milled and of transformed bcc phases when annealed.

4.4 ^{119}Sn Mössbauer spectra

4.4.1 ^{119}Sn Mössbauer spectra of equilibrium solid solutions of Sn in B2 FeCo

Only a few ^{119}Sn Mössbauer studies were devoted to FeCo [26-28]. Ordered B2 FeCo and near-equiatomic FeCo were doped with at most 1 at.% of ^{119}Sn enriched tin. The spectra are composed of a magnetically split component and of a central component which appears as a (weak [27]) "doublet". The HMF's of Sn atoms on the Co sublattice, with eight Fe nearest neighbors in perfectly ordered FeCo, are large, B_S(Co) ~23-25 T, with a slight decrease of the field when the cobalt content increases beyond 50 at.% (table 1). By contrast, B_S(Fe) is rather close to zero, but definitely different from zero, for Sn atoms on the Fe sublattice, with eight Co nearest neighbors in perfectly ordered FeCo (table 1). From the relative intensities of the two spectral components, Sn is

concluded to occupy preferentially sites of the Co sublattice in a sample annealed for weeks at a succession of decreasing temperatures down to 673K and then quenched [27]. A long-range order parameter S close to 1 and the low Sn content account for well-resolved and narrow lines of the magnetic sextet seen for instance in figure 1 of [26]. The "doublet" intensity was found to increase by a factor of ~5 when a ^{119}Sn doped-FeCo sample was annealed for 15 days at 873K and quenched [27].

From a collection of ^{119}Sn HMF's measured at 77K, Delyagin and Kornienko [58] proposed a relation which expresses mean HMF's $<B_S>$ of diamagnetic Sn in various ferro- and antiferromagnetic bcc alloys: $<B_S>$ (T) $=-21.8<\mu_1>+0.9<\mu_2>+16.5<\mu>$. It includes the magnetic moments (in μ_B) $<\mu_k>$ of atoms of the first two coordination shells around the considered tin atom (k=1,2) and an additional contribution from more remote shells whose total effect is taken to be proportional to the average magnetic moment of the alloy, $<\mu>$. As the Curie temperature of B2 FeCo is high, T_C=1253K [59], the decrease of Sn HMF's between 0K and RT is only of the order of 10% [27] which is the expected precision of the estimates obtained from this semi-empirical model. In other words, the precise values of the measurement temperatures of the HMF's between 0K and RT don't need to be considered to get the estimates given below. At 0K, the mean magnetic moments $<\mu_{Fe}>$ are 3.02 μ_B and 2.92 μ_B in disordered A2 FeCo and in ordered B2 FeCo respectively while the moments $<\mu_{Co}>$ are respectively 1.81 μ_B and 1.62 μ_B [64-66]. The previous model yields then $<B_S(Co)>$= -23.6 T and $<B_S(Fe)>$ =+2.5 T.

Table 1 compares mean ^{119}Sn HMF's measured at RT in various $Fe_xCo_ySn_{100-x-y}$ alloys. The ^{119}Sn HMF's in bcc $Fe_{100-z}Sn_z$ alloys reach their maximum for dilute alloys and decrease steadily when z increases [38-39]. The maximum HMF in table 1 is by far the field of tin atoms on the Co sublattice of B2 FeCo. The corresponding mean fields are expected to be smaller for Sn-rich near-equiatomic Fe-Co alloys than they are for dilute alloys as explained below.

4.4.2 ^{119}Sn Mössbauer spectra of annealed $Fe_{53.3-0.6x}Co_{46.7-0.4x}Sn_x$

The HMFD's obtained from ^{119}Sn spectra of annealed alloys differ strongly from their counterparts in as-milled alloys which are approximatively Gaussians with values of

Table 1:

Mean ^{119}Sn hyperfine magnetic fields, $\langle B_S \rangle$ (T), measured at RT in $Fe_xCo_ySn_{100-x-y}$ alloys (preparation method: LH= melting+cooling+heat treatment, MA=mechanical alloying, SSD=solid state diffusion).

Composition (at.%)	$\langle B_S \rangle$ (T) [reference]	preparation, structure
$Fe_{99.5}Sn_{0.5}$	7.89 [60]	LH, bcc
$Fe_{92}Sn_8$	5.9 [30]	MA, bcc
$Fe_{82}Sn_{18}$	4.5 [30]	MA, bcc
$Fe_{80}Sn_{20}$	4.0 [39]	MA, bcc
Fe_3Sn	8.3 [61]	SSD, D019
$Co_{98}Sn_2$	3.6 [62]	quench, hcp
$Co_{99.5}Sn_{0.5}$	1.7 [62-63]	LH, fcc
B2 alloys	Co sublattice	preparation, structure
$Fe_{49.9}Co_{49.9}Sn_{0.2}$	25.2* [26]	LH, B2
$Fe_{49.5}Co_{49.5}Sn_1$	25.3 [27]	LH, B2
$Fe_{47.3}Co_{52.4}Sn_{0.3}$	23.1 [28]	LH, B2
B2 alloy	Fe sublattice	preparation, structure
$Fe_{49.5}Co_{49.5}Sn_1$	0.7* [26]	LH, B2

** HMF's measured at 77K mentioned to be hardly altered between 77K and RT*

$\langle B_S(x) \rangle$ and $B_M(x)$ both close to 10 T (figure 9 left and figure 11). We note in passing that the previous semi-empirical relation may be applied to bcc $Fe_{46}Co_{42}Sn_{12}$ alloy assuming no changes of the mechanisms which determine the tin hyperfine fields. The moments $\langle \mu_{Fe} \rangle$ and $\langle \mu_{Co} \rangle$ are simply replaced by the mean magnetic moment per transition metal atom, $\langle \mu_T \rangle$ =2.05 μB, which is measured at 5K (figure 3 of [31]). The predicted value, $\langle B_S(x=12) \rangle$=-9 T, is in good agreement with the experimental result (9.5 T [30]) as signs cannot be determined from Mössbauer spectra in zero applied magnetic field.

Intense peaks emerge in the ^{119}Sn hyperfine magnetic field distributions at RT at field values of ~20 T for any $x \leq 21$ as expected when annealed bcc $Fe_{53.3-0.6x}Co_{46.7-0.4x}Sn_x$

phases order to a B2 structure (figures 8 and 10). To get rid of a significant effect of a lower Curie temperature on the RT spectra, ^{119}Sn Mössbauer spectra were recorded at 15K for x=21 and 26. The associated HMFD's are shown in figure 10 (right). Although the broad magnetic component shifts downwards when x increases, it is still centered on a HMF significantly larger than 10 T for x=26.

Let $P_{Co}(x,\mathbf{n})$, where $\mathbf{n}=(n_{Fe}(1),n_{Co}(1),n_{Sn}(1),\ n_{Fe}(2),n_{Co}(2),n_{Sn}(2),..)$, be the probability that a Sn atom on the Co sublattice has $n_X(i)$ atoms of type X (X=Fe,Co,Sn) on its i^{th} coordination shell for a tin content of x. The additional dependence of $P_{Co}(x,\mathbf{n})$ on long-range order is left implicit. From the semi-empirical model considered above [58], it suffices to consider i=1,2. Every number $n_X(i)$ ranges then between 0 and 8 and between 0 and 6 for i=1,2 respectively. In perfectly ordered B2 FeCo (S=1) [25], a single environment exists around Sn atoms in the dilute case, i.e. $P_{Co}(\sim 0,\mathbf{n})\approx 1$ for $\mathbf{n}=(8,0,0,0,6,0)$ and 0 else. The latter distribution broadens when the LRO parameter decreases. For a random distribution of Fe and Co atoms in a dilute alloy of Sn in $Fe_{50}Co_{50}$, it comes $P_{Co}\left(\sim 0,\mathbf{n}_r\right)\approx\binom{8}{n_{Fe}(1)}\times\binom{6}{n_{Co}(2)}\times\left(\frac{1}{2}\right)^{14}$ where $\binom{m}{k}$ is a binomial coefficient, $\mathbf{n}_r=(n_{Fe}(1),\ 8\text{-}n_{Fe}(1),0,\ 6\text{-}n_{Co}(2),n_{Co}(2),0)$ and $n_{Fe}(1)=0,..,8,\ n_{Co}(2)=0,..,6$.

In contrast to narrow lines of Mössbauer spectra of Sn diluted in FeCo with S≈1 [26], the broad lines of the magnetic component at ~20 T (figures 8 and 10) arise mainly from a variety of atomic environments of Sn atoms on the Co sublattice as quantified by the probability distribution $P_{Co}(x,\mathbf{n})$ discussed above. Part of line broadening comes from ultrafine ordered domains which result in a high density of antiphase boundaries. The environments of Sn atoms located in these boundaries are perturbed as compared to those of Sn atoms inside domains. The evolution with x of $<B_S(x)>$ and of $B_M(x)$ is shown in figure 11 (right). Their slow decrease with tin content ($x \leq 21$) is first caused by a decrease of the Curie temperature. An additional effect on the Sn HMF's comes from a deviation from 1 of the ratio of Fe content to Co content (table 1, [28]).

The mean and the width of the HMFD $P_S(B)$ are related to the characteristics of the distribution $P_{Co}(x,\mathbf{n})$ which evolve both when x increases and when the long-range order parameter decreases. The maximum value of the LRO parameter in various nanocrystalline materials is reduced typically to ~80% of the value expected at equilibrium in bulk samples ([35] and references therein).

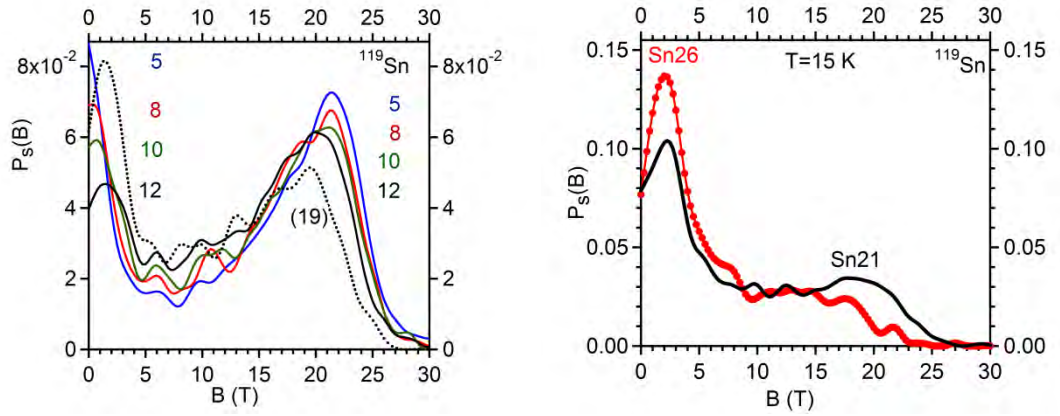


Figure 10 - ^{119}Sn hyperfine magnetic field distributions of as-milled (10h) $Fe_{53.3-0.6x}Co_{46.7-0.4x}Sn_x$ annealed at 673K for 15h (right) : (left) distributions at RT for the indicated values of x) and (right) distributions at 15K for x=21, 26. (color online).

It is however difficult to describe in detail the dependence of the Sn HMF's on their environments as no reliable theoretical model exists to date. The model described in section 4.4.1 is semi-empirical and enables only to estimate mean fields once average magnetic moments of the first coordination shells are known.

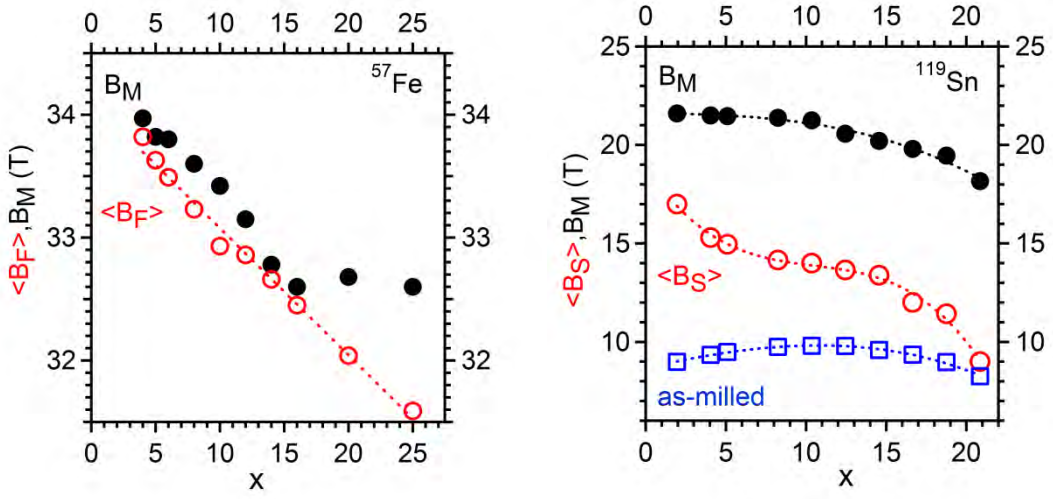


Figure 11 - As-milled (10h) $Fe_{53.3-0.6x}Co_{46.7-0.4x}Sn_x$ annealed at 673K for 15h: ^{57}Fe (left) and ^{119}Sn (right) HMF's at RT: $< B_F >$ and $< B_S >$ (empty circles), and B_M (solid circles) as a function of x. For comparison, $< B_S >$ is shown for as-milled alloys (right, empty squares) (the associated B_M almost coincides with it). (color online).

Ab initio calculations of the ^{57}Fe hyperfine magnetic field in B2 FeCo predict fields whose magnitudes are smaller than the experimental fields by ~7.5 T or ~6 T according to the method used [67]. This constitutes an additional difficulty for trustworthy

calculations of ^{119}Sn HMF's in dilute alloys of Sn in B2 FeCo. Presently, it seems hopeless to account theoretically for ^{119}Sn HMFD's in the concentrated and partly disordered Fe-Co-Sn alloys we studied and thus to extract from them a detailed information about short-range order. Fortunately, mean HMF's and the two components of HMFD's carry valuable information about the existence of a long-range ordered B2 phase in these alloys and about the repartition of tin between its two sublattices (next section).

To conclude ^{119}Sn Mössbauer spectra, with a broad component at HMF's much larger than 10 T, prove unambiguously that annealed bcc $Fe_{53.3-0.6x}Co_{46.7-0.4x}Sn_x$ order to a B2 type structure in agreement with neutron diffraction results.

4.4.3 Evolution with x of the repartition of tin on the Fe and Co sublattices of the B2 phase

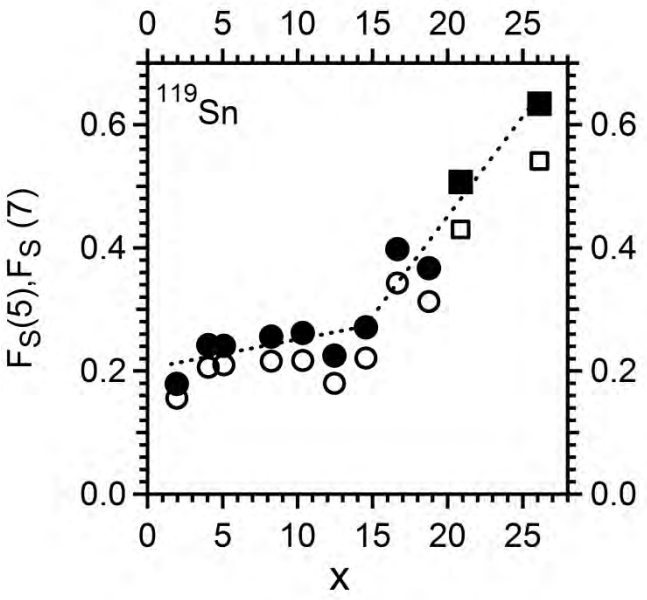


Figure 12 - As-milled (10h) $Fe_{53.3-0.6x}Co_{46.7-0.4x}Sn_x$ annealed at 673K for 15h: Fraction at RT of ^{119}Sn atoms whose HMF's are either less or equal to 5 T (empty circles) or less or equal to 7 T (solid circles), as a function of x for $x \leq 19$. The values at 15K are plotted for x=21, 26 (empty squares for 5 T and solid squares for 7 T). The dashed lines are guides to the eye.

An additional change takes place in the alloys we studied. The intensities of the central component for x=19, 21, 26 are indeed enhanced with respect to those observed for $x \leq 12$ (figure 10). To make it more quantitative, we calculated, as a function of x, the fractions of ^{119}Sn atoms whose hyperfine magnetic fields are either less or equal to 5 T ($F_S(5)$) or less

or equal to 7 T ($F_S(7)$) (figure 12). These fractions are fairly well representative of the fraction of tin atoms whose number of Co neighbors is large, either equal to eight or close to it (section 4.2). The values of $F_S(5)$ and of $F_S(7)$ at 15K are used for x=21, 26. In any case, the latter are equal to or smaller than their corresponding values at RT. Both $F_S(5)$ and of $F_S(7)$ display a change of slope at ~15 at.% (figure 12). This suggests that short-range order of tin atoms evolves with x. In annealed alloys, Sn atoms tend then to have much more Fe neighbors than Co neighbors for x below ~15 at.% and vice versa for x beyond ~15 at.%.

4.5 The extent of B2 ordering in Fe-Co-Sn alloys

The occurrence of metastable B2 ordering is established with certainty from neutron diffraction patterns and ^{119}Sn Mössbauer spectra in $Fe_{53.3-0.6x}Co_{46.7-0.4x}Sn_x$ for $x \leq 26$. As discussed in section 1.1, it exists too for $Fe_{50}Co_{25}Sn_{25}$ and possibly for other alloy compositions such as $Fe_{75-x}Co_xSn_{25}$ ($0 \leq x \leq 75$). Combining all results, we conclude that long-range order of B2 type exists most likely over a significant concentration range for Sn-rich Fe-Co-Sn alloys. This conclusion is not really surprising for the present alloys when their tin contents are small. However, the fact that equiatomic FeCo orders in that way does not imply that bcc $Fe_{53.3-0.6x}Co_{46.7-0.4x}Sn_x$ solid solutions, with a very high degree of supersaturation, have to order similarly. The association of two 3d elements with an sp element plays without doubt a role in the observed ordering.

5. Conclusions

Mechanosynthesized ternary alloys with overall composition $Fe_{53.3-0.6x}Co_{46.7-0.4x}Sn_x$ ($2 \leq x \leq 34$), are composed of a supersaturated bcc phase for x<~15 at.%. For larger values of x, as-milled powders consist primarily of a bcc phase with steadily increasing tin contents and of extra phases which include hexagonal $(Fe,Co)_3Sn_2$. The tin content which can be really dissolved in near-equiatomic bcc Fe-Co alloys in our milling conditions appears thus to be much closer to 26 at.% than to 15 at.%.

Neutron diffraction patterns and ^{119}Sn Mössbauer spectra prove unambiguously that the bcc phases of as-milled alloys transform into B2 phases for $2 \leq x \leq 26$ when annealed at 673K. Beyond long-range order, ^{57}Fe and ^{119}Sn Mössbauer spectra provides evidence

that the previous tin content, ~15 at.%, marks too the separation between domains with different repartitions of tin atoms between the two sublattices of the B2 structure.

Combining our results with published results, we are led to conclude that metastable B2 alloys are formed over a significant concentration range in Sn-rich ternary Fe-Co-Sn alloys.

Acknowledgements

This paper is dedicated to the memory of Alain Reza Yavari (SIMAP, Grenoble INP). The financial support of the bilateral Portuguese-French program FCT-CNRS is gratefully acknowledged. We thank ILL for the provision of neutron beam time. We thank P.M. Gordo (Physics Department, University of Coimbra), A. Ramalho (Department of Mechanical Engineering, University of Coimbra) and P. Delcroix (Université de Lorraine) for providing assistance in some aspects of the study. We thank Dr. R. A. Brand (Universität Duisburg-Essen) for useful discussions.

References

[1] Sourmail T (2005) Near equiatomic FeCo alloys: constitution, mechanical, magnetic properties Prog Mater Sci 50: 816-880

[2] Neumayer M, Fähnle M (2001) Atomic defects in FeCo: stabilization of the *B*2 structure by magnetism. Phys. Rev. B 64: 132102 (4 pages)

[3] Drautz R, Díaz-Ortiz A, Fähnle M, Dosch H (2004) Ordering and magnetism in Fe-Co: dense sequence of ground-state structures, Phys. Rev. Lett. 93: 067202 (4 pages)

[4] Hasegawa H, Pettifor DG (1983) Microscopic theory of the temperature-pressure phase diagram of iron, Phys. Rev. Lett. 50: 130-133

[5] Fultz B (1991) Kinetics of short-range and long-range B2 ordering in FeCo. Phys Rev B 44: 9805-9811

[6] Yin M, Hasier J, Nash P (2016) A review of phase equilibria in Heusler alloy systems containing Fe, Co or Ni. J Mater Sci 51: 50-70

[7] Buschow KHJ, van Engen PG (1983) Note on the magnetic and magneto-optical properties of Ni_2In type 3d transition metal compounds. Phys Stat Sol (a) 76: 615-620

[8] Singh VK, Singh M, Bhan S (1982) Metastable Phases in $Fe_{75}Sn_{25}$-$Co_{75}Sn_{25}$ Alloys. Phys Stat Sol (a) 74: K115-K117

[9] Schluckebier G, Wachtel E, Predel B (1980) A New Intermetallic Phase in the Co-Sn System. Z Metallkde 71: 456-460

[10] Zhang W, Jiko N, Mibu K, Yoshimura K (2005) Effect of substitution of Mn with Fe or Cr in Heusler alloy of Co_2MnSn. J Phys: Condens Matter 17: 6653-6662

[11] Yin M, Chen S, Nash P (2013) Enthalpies of formation of selected Co_2YZ Heusler compounds. J Alloys Compd 577: 49-56

[12] Duan J, Kou X (2013) Effect of Current Density on the Microstructure and Magnetic Properties of Electrodeposited Co_2FeSn Heusler Alloy. J Electrochem Soc 160: D471-D475

[13] Watanabe N, Sano K, Tasugi N, Yamaguchi T, Yamamoto A, Ueno M, Sumiyoshi R, Arakawa T, Koiwa I (2015) Preparation of Co_2FeSn Heusler alloys by electrodeposition method. APL Mater 3: 041804 (5 pages)

[14] Li T, Duan J, Yang C, Kou X (2013) Synthesis, microstructure and magnetic properties of Heusler Co_2FeSn nanoparticles. Micro Nano Lett IET 8:143-146

[15] Tanaka M A, Ishikawa Y, Wada Y, Hori S, Murata A, Horii S, Yamanishi Y, Mibu K, Kondou K, Ono T, Kasai S (2012) Preparation of Co_2FeSn Heusler alloy films and magnetoresistance of Fe/MgO/Co_2FeSn magnetic tunnel junctions. J Appl Phys 111: 053902 (4 pages)

[16] Gaffet E, Bernard F, Niepce JC, Charlot F, Gras C, Le Caër G, Guichard JL, Delcroix P, Mocellin A, Tillement O (1999) Some recent developments in mechanical activation and mechanosynthesis, J. Mater. Chem. 9 : 305–314

[17] Suryanarayana C (2001) Mechanical alloying and milling. Prog Mater Sci, 46: 1-184

[18] Bellon P, Martin G (1996) Driven alloys, Solid State Phys. 50: 189-331

[19] Pochet P, Tominez E, Chaffron L, Martin G (1995) Order-disorder transformation in Fe-Al under ball milling. Phys. Rev. B 52: 4006-4016

[20] Brüning R, Samwer K, Kuhrt C, Schultz L (1992) The mixing of iron and cobalt during mechanical alloying. J Appl Phys 72: 2978-2983

[21] Elkakouli R, Grosbras M, Dinhut JF (1995) Mechanical and magnetic properties of nanocrystalline FeCo alloys produced by mechanical alloying, NanoStruct Mater 5: 733-743

[22] Sorescu M, Grabias A (2002) Structural and magnetic properties of Fe50Co50 system, Intermetallics 10: 317-321

[23] Moumeni H, Alleg S, Grenèche JM (2005) Structural properties of Fe50Co50 nanostructured powder prepared by mechanical alloying, J Alloys Compd 386: 12-19

[24] Garroni S, Delogu F, Mulas G, Cocco G (2007) Mechanistic inferences on the synthesis of $Co_{50}Fe_{50}$ solid solution by mechanical alloying. Scripta Mater 57: 964-967

[25] Loureiro JM, Malaman B, Costa BFO, Le Caër G, Khomchenko VA, Das S, Amaral VS (2011) Comparison of disorder induced by annealing and quench and by ball-milling in B2 FeCo, Phys. Stat. Sol. (c) 8: 3087-3090

[26] Delyagin NN, Kornienko EN (1971) Hyperfine magnetic fields for ^{119}Sn atoms in ferromagnetic CoFe. Sov Phys Solid State 13: 1254-1255

[27] Huffman GP, Dunmyre GR (1973) Hyperfine fields at ^{119}Sn nuclei in ordered Fe-Co and γ-Fe-Mn. CoFe.AIP Conf Proc 10: 1361-1364

[28] Campbell CCM, Schaf J, Zawislak FC (1978) Magnetic hyperfine fields at Fe, Cd and Sn sites in an FeCo alloy. J Magn Magn Mater 8: 112-118

[29] Loureiro JM, Costa BFO, Le Caër G (2012) Mechanosynthesis of supersaturated solid solutions of Sn in near-equiatomic bcc FeCo. J Alloys Compd 536S: S31-S34

[30] Loureiro JM, Costa BFO, Le Caër G, Malaman B (2013) Mechanically driven dissolution of Sn in near-equiatomic bcc FeCo. Solid State Phenom 194: 187-193

[31] Loureiro JM, Costa BFO, Malaman B, Le Caër G, Das S, Amaral VS (2014) Formation stages of bcc (Fe44Co44)Sn12 extended solid solution by mechanical alloying. J Alloys Compd 615: S559-S563

[32] Leonova EA, Delcroix P, Le Caër G, Kaloshkin SD, Baldokhin YuV (2003) Reordering of a Ni_2MnSn Heusler Alloy after Disordering in a Planetary Ball Mill. J Metastab Nanocryst 15-16: 239-244

[33] Cahn RW (1999) Disordering and reordering of mechanically milled superlattice alloys. Bull Mater Sci 22: 175-180

[34] Suriñach S, Amils X, Gialanella S, Lutterotti L, Baró MD (1997) Kinetics of reordering in a nanograined FeAl alloy. Mater Sci Forum 235-238: 415-420

[35] Ziller T, Le Caër G, Isnard O, Cénédèse P, Fultz B (2002) Metastable and transient states of chemical ordering in Fe-V nanocrystalline alloys. Phys Rev B 65: 024204 (14 pages)

[36] Evain M (1992) U-FIT A cell parameter refinement program, internal report, Institut des Matériaux Jean Rouxel, Nantes, France

[37] Le Caër G, Dubois JM (1979) Evaluation of hyperfine parameter distributions from overlapped Mössbauer spectra of amorphous alloys. J Phys E 12 : 1083-1090

[38] Cabrera AF, Sánchez FH, Mendoza Zélis LA (1996) Time and composition dependence of mechanical alloying of $Fe_{1-x}Sn_x$. Phys Rev B 53: 8378-8385

[39] Yelsukov EP, Voronina EV, Konygin GN, Barinov VA, Godovikov SK, Dorofeev GA, Zagainov AV (1997) Structure and magnetic properties of $Fe_{100-x}Sn_x$ ($3.2 < x < 62$) alloys obtained by mechanical milling. J Magn Magn Mater 166 : 334-348

[40] Dorofeev GA, Elsukov EP (2000) Thermodynamic modeling of mechanical alloying in the Fe–Sn system. Inorg Mater 36: 1228-1234

[41] Wang XL, Chen H, Bai J, Han WQ (2012) $CoSn_5$ Phase: Crystal Structure Resolving and Stable High Capacity as Anodes for Li Ion Batteries J Phys Chem Lett 3: 1488-1492

[42] Di LM, Zhou GF, Bakker H (1993) Atomic disorder, phase transformation, and phase restoration in Co_3Sn_2. Phys Rev B 47: 4890-4895

[43] Xie J, Zhao XB, Cao GS, Tu JP (2007) Electrochemical performance of nanostructured amorphous Co_3Sn_2 intermetallic compound prepared by a solvothermal route. J Power Sources 164: 386-389

[44] Tamura N, Fujimoto M, Kamino M, Fujitani S (2005) Mechanical stability of Sn–Co alloy anodes for lithium secondary batteries. Electrochim Acta 49: 1949-1956

[45] Guilmin P, Guyot P, Marchal G (1985) Amorphization of crystalline cobalt and tin multilayers by solid state reaction at room temperature. J Phys Colloque Paris, 46: C8-485-C8-489

[46] Gaffet E, Anglezio J C, Bigot J, Martin G (1988) Amorphization by solid state diffusion in granular system. J Less-Common Met 140: 49-55

[47] Arzhnikov A K, Dobysheva L V, Elsukov E P, Zagainov A V (1996) Concentration dependence of the magnetization and the Curie temperature in disordered Fe-M alloys (M=AI, Si, Sn). JETP 83: 623-627

[48] Kovacheva D, Ruskov T, Krystev P, Asenov S, Tanev N, Mönch I, Koseva R, Wolff U, Gemming T, Markova-Velichkova M, Nihtianova D, Arndt, K-F (2012) Synthesis and characterization of magnetic nano-sized Fe_3O_4 and $CoFe_2O_4$. Bulg Chem Commun 44: 90-97

[49] Rodmacq B, Piecuch M, Janot Chr, Marchal G,, Mangin Ph (1980) Structure and magnetic properties of amorphous Fe_xSn_{1-x} alloys. Phys Rev B 21: 1911-1923

[50] Ma E, Atzmon M (1991) Calorimetric Evidence for Polymorphous Constraints on Metastable Zr-Al Phase Formation by Mechanical Alloying. Phys Rev Lett 67: 1126-1129

[51] Schilling P J, Palshin V, Tittsworth R C, He J H, Ma E (2003) Overlapping solid solubility in mechanically alloyed Fe-Ni and Fe-Cu. Phys Rev B 68: 224204 (5 pages)

[52] Fultz B, Howe JM (2013) Transmission Electron Microscopy, Diffractometry of Materials. Springer Verlag, Berlin

[53] Loureiro J M, Batista A C, Khomchenko V A, Costa B F O, Le Caër G (2011) Order-disorder phenomena from X-ray diffraction in FeCo alloys annealed and ground at high energy. Powder Diffr 26: 267-272

[54] Chapink FW (2001) Ordered states in ternary B2-type intermetallic alloys including vacancies. Phil Mag A 81: 883-901

[55] Eymery JP, Moine P (1978) Ordre atomique et spectrométrie Mössbauer dans l'alliage Fe-Co équiatomique. J Phys Lett-Paris 39: L23-L28

[56] deMayo, B (1981) Atomic ordering transition in FeCo. Phys Rev B 24: 6503-6507

[57] Hamdeh HH, Fultz B, Pearson DH (1989) Mössbauer spectrometry study of the hyperfine fields and electronic structure of Fe-Co alloys. Phys Rev B 39: 11233-11240

[58] Delyagin NN, Kornienko EN (1972) Magnetic hyperfine interaction for tin atoms in metallic ferro- and antiferromagnets with bcc structure. Sov Phys JETP 34: 1036-1041

[59] Sundar RS, Deevi SC (2005) Soft magnetic FeCo alloys: alloy development, processing, and properties. Int Mater Rev 50: 157-192

[60] Price DC (1974) The temperature dependence of the hyperfine interactions at ^{119}Sn in iron. J Phys F: Metal Phys 4: 639-662

[61] Djéga-Mariadassou C, Lecocq P, Trumpy G, Träff J, Østergaard P (1966) Mössbauer study on FeSn and Fe_3Sn. Nuovo Cimento 46 B: 35-45

[62] Jain AP, Cranshaw TE (1967) Anomalous temperature dependence of the hyperfine fields at Sn in cobalt. Phys Lett 25A: 421-422

[63] Cranshaw TE (1969) Anomalous temperature dependence of the hyperfine field at ^{119}Sn in Co. J Appl Phys 40: 1481-1483

[64] Bardos D I (1969) J Appl Phys Mean Magnetic Moments in bee Fe-Co Alloys. 40: 1371-1372

[65] Kulkova SE, Valujsky DV, Sam Kim Jai, Lee Geunsik, Koo YM (2002) The electronic properties of FeCo, Ni_3Mn and Ni_3Fe at the order–disorder transition. Physica B 322: 236-247

[66] Bhatia ML (2010) Magnetic moments in the Fe-Co system. Curr Sci India 99: 785-790

[67] Samara Q, Al-Sharif AI, Mahmood SH (2006) On the magnetic properties and hyperfine fields in Fe-containing alloys: A theoretical study. Phys. Stat. Sol. (c) 3 : 3285–3291